Off-fault long-term damage: A condition to account for generic, triangular earthquake slip profiles,

F. Cappa, C. Perrin, I. Manighetti, E. Delor

▶ **To cite this version:**

F. Cappa, C. Perrin, I. Manighetti, E. Delor. Off-fault long-term damage: A condition to account for generic, triangular earthquake slip profiles,. Geochemistry, Geophysics, Geosystems, 2014, 15 (4), pp.1476-1493. 10.1002/2013GC005182 . hal-00996403

HAL Id: hal-00996403
https://hal.science/hal-00996403

Submitted on 10 Jan 2022

HAL is a multi-disciplinary open access archive for the deposit and dissemination of scientific research documents, whether they are published or not. The documents may come from teaching and research institutions in France or abroad, or from public or private research centers.

L'archive ouverte pluridisciplinaire **HAL**, est destinée au dépôt et à la diffusion de documents scientifiques de niveau recherche, publiés ou non, émanant des établissements d'enseignement et de recherche français ou étrangers, des laboratoires publics ou privés.

AGU PUBLICATIONS

Geochemistry, Geophysics, Geosystems

RESEARCH ARTICLE
10.1002/2013GC005182

Key Points:
- Off-fault long-term damage controls earthquake slip
- Rupture models with along-fault variability in long-term damage properties reproduce generic shape of natural earthquake slip profiles
- Coseismic strain dissipated off the main fault is significant and occurring over large distances

Supporting Information:
- README
- Tables S1-S2

Correspondence to:
F. Cappa,
cappa@geoazur.unice.fr

Citation:
Cappa, F., C. Perrin, I. Manighetti, and E. Delor (2014), Off-fault long-term damage: A condition to account for generic, triangular earthquake slip profiles, *Geochem. Geophys. Geosyst.*, *15*, 1476–1493, doi:10.1002/2013GC005182.

Received 3 DEC 2013
Accepted 4 APR 2014
Accepted article online 8 APR 2014
Published online 29 APR 2014

Off-fault long-term damage: A condition to account for generic, triangular earthquake slip profiles

Frédéric Cappa[1], Clément Perrin[1], Isabelle Manighetti[1], and Elodie Delor[1]

[1]Université de Nice Sophia-Antipolis, CNRS, IRD, Observatoire de la Côte d'Azur, Geoazur UMR 7329, Valbonne, France

Abstract Natural earthquake slip profiles have a generic triangular shape which the available rupture dynamics models fail to reproduce. Long-term faults are embedded in long-damaged crustal material, and the properties of the long-term damage vary both across and along the faults. We examine the effects of the predamaged state of the medium on the earthquake slip distributions. We simulate long-term damage by the decrease in the elastic modulus of the medium around the fault. We model the dynamic crack-like rupture of a slip-weakening planar, right-lateral strike-slip fault, and search which geometries and elastic properties of the long-term damage produce a triangular slip profile on the rupture. We find that such a profile is produced only when a laterally heterogeneous preexisting damage zone surrounds the ruptured fault. The highest on-fault slip develops in the most compliant region of the damage zone, and not necessarily above the earthquake hypocenter. The coseismic slip decreases in zones of stiffer damage. The amount of coseismic slip dissipated in the damage zone is large, at least 25–40% of maximum on-fault slip, and can occur over large distances from the fault. Our study thus emphasizes that off-fault preexisting damage should be considered for an accurate description of earthquake ruptures. It also motivates a reformulation of the available earthquake source inversion models since most of them do not include the inelastic deformations that occur in the near field of the earthquake ruptures.

1. Introduction

The aim of this paper is to explain slip distributions on earthquake ruptures. Based on ~100 slip distributions for natural earthquakes, *Manighetti et al*. [2005] showed that coseismic slip-length profiles are typically triangular and asymmetric, regardless of rupture length, earthquake magnitude ($M_w \geq \sim 6.0$), slip mode, location, and geological context (Figure 1a). The triangular envelope shape of coseismic slip profiles is thus a generic property of earthquakes, that is, an intrinsic, common property that must result from the physics of the dynamic rupture process [*Noda et al*., 2013], not from site-dependent or fault-specific factors. Therefore, it is important to understand how those triangular slip distributions are formed; classical models of crack-like ruptures expanding in a self-similar manner on a planar fault embedded in a linear elastic medium predict an elliptical characteristic slip profile [*Andrews*, 2005] and hence fail to reproduce the observed triangular form.

Based on prior studies of long-term faults ($\geq 10^4 - 10^6$ years) and related cumulative damage [*Manighetti et al*., 2001, 2004] and on long-standing knowledge of earthquake energy partitioning [e.g., *Kostrov*, 1974; *Dahlen*, 1977; *Aki and Richards*, 2002; *Tinti et al*., 2005; *Kanamori and Rivera*, 2006], *Manighetti et al*. [2005] suggested that the smooth linear decrease in earthquake slip might result from coseismic inelastic deformation—referred to as "coseismic damage"—affecting a large part of the medium as the rupture is developing. An increasing number of observations support this suggestion, in which significant coseismic failure and strain occurs around large earthquake ruptures [*Fialko et al*., 2002; *Fialko*, 2004; *Hamiel and Fialko*, 2007; *Cochran et al*., 2009; *Fielding et al*., 2009]. Experimental and theoretical models have also been developed recently to examine whether off-fault coseismic damage could emerge from the dynamic rupture process [*Harris and Day*, 1997; *Lyakhovsky et al*., 1997; *Yamashita*, 2000; *Poliakov et al*., 2002; *Dalguer et al*., 2003; *Rice et al*., 2005; *Andrews*, 2005; *Ben-Zion and Shi*, 2005; *Ando and Yamashita*, 2007; *Bhat et al*., 2007; *Templeton and Rice*, 2008; *Biegel et al*., 2008; *Viesca et al*., 2008; *Dunham and Rice*, 2008; *Duan and Day*, 2008; *Ma*, 2008; *Sammis et al*., 2009; *Dieterich and Smith*, 2009; *Finzi et al*., 2009; *Bhat et al*., 2010; *Biegel et al*., 2010; *Ma and Andrews*, 2010; *Shi et al*., 2010; *Hok et al*., 2010; *Savage and Cooke*, 2010; *Dunham et al*., 2011a, 2011b; *Xu et al*., 2012a, 2012b; *Ngo et al*., 2012; *Suzuki*, 2012; *Xu and Ben-Zion*, 2013; *Gabriel et al*., 2013]. Although they

© 2014. American Geophysical Union. All Rights Reserved.

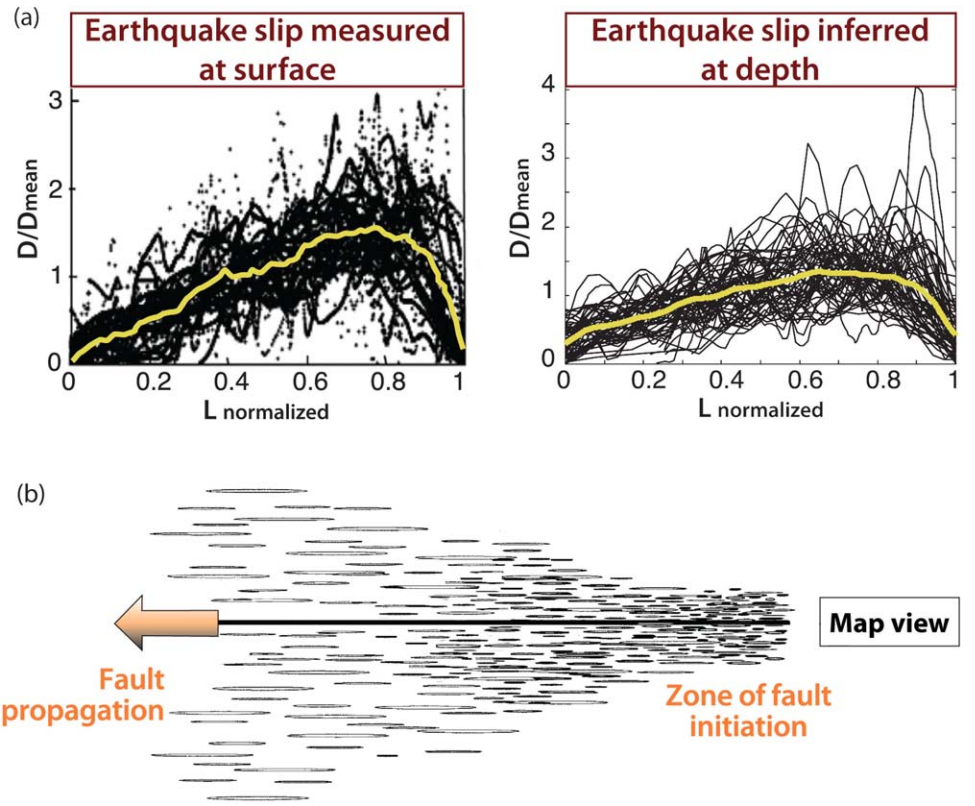

Figure 1. (a) Earthquake slip profiles (normalized) measured at the ground surface (left) and inferred at depth from earthquake source inversion models (right) for about 50 different historical earthquakes (~100 different slip profiles among surface and depth) with different rupture lengths, magnitudes ($M_w \geq 6$), slip modes, and locations worldwide [from *Manighetti et al.*, 2005]. The generic shape of the earthquake slip profiles is well represented by the average curve in yellow calculated for each data set. (b) Schematic long-term fault architecture deduced from geological observations [from *Manighetti et al.*, 2004]. The fault plane (presented here in map view, as a solid horizontal line) is surrounded with a long-term damage zone, made of multiple small fractures and faults (here sketched as narrow, elongated ellipses either side of the fault) that formed during the fault evolution. The intensity of damage, revealed here through the density of fractures, is higher in the region where the fault originally initiated and reduced in the direction of fault lengthening and hence of fault decreasing age. The total width of the damage zone increases in the direction of long-term fault lateral propagation. We model in Figure 7b this form of triangular damage zone.

are based on different formalisms, all these models confirm that significant coseismic off-fault damage does develop during the earthquake rupture, with this development markedly affecting the mode and properties (i.e., speed and directivity) of the dynamic rupture and the seismic radiation. However, none of these studies have addressed the question of earthquake slip profiles; either the slip distributions that emerge from the experiment or modeling are not examined [*Sammis et al.*, 2009; *Hok et al.*, 2010; *Suzuki*, 2012; *Xu and Ben-Zion*, 2013; *Gabriel et al.*, 2013] or they are examined yet found to be different from natural, generic slip profiles [*Andrews*, 2005; *Dunham and Rice*, 2008; *Templeton and Rice*, 2008; *Dieterich and Smith*, 2009; *Savage and Cooke*, 2010; *Griffith et al.*, 2010; *Dunham et al.*, 2011a, 2011b; *Xu et al.*, 2012a].

We suggest that the later discrepancy is due, at least in part, to the fact that most theoretical models simulate the rupture in a medium whose predamage state is not fully appropriate. As recognized for long by geologists, the growth and lateral lengthening of faults over geological time leaves behind the passage of their tips a wake of fractured, damaged rocks [e.g., *Scholz et al.*, 1993]. Even though various healing processes might occur at specific periods of the earthquake cycle and during the evolution of the fault [e.g., *Brantley et al.*, 1990; *Moore et al.*, 1994; *Vidale and Li*, 2003; *Schaff and Beroza*, 2004; *Brenguier et al.*, 2008; *Mitchell and Faulkner*, 2009], part of the damage (i.e., cracks and faults) is persistent, so that rock damage is cumulative and permanent [e.g., *Chester and Chester*, 1998; *Li et al.*, 1998; *Sibson*, 2003; *Manighetti et al.*, 2004; *Dor et al.*, 2008; *Mitchell and Faulkner*, 2009; *Barbot et al.*, 2009; *Cochran et al.*, 2009; *Hearn and Fialko*, 2009; *Savage and Cooke*, 2010; *Savage and Brodsky*, 2011; *Griffith et al.*, 2012; *Smith et al.*, 2013]. Furthermore, the cumulative, long-term damage is heterogeneous, varying both across and along the fault; across the fault, the damage "intensity" (commonly taken as the crack density) decreases away from the fault [e.g., *Chester and Logan*, 1986; *Vermilye and Scholz*, 1998; *Faulkner et al.*, 2006; *Wechsler et al.*, 2009; *Mitchell and*

© 2014. American Geophysical Union. All Rights Reserved.

Faulkner, 2009; *Savage and Brodsky*, 2011; *Smith et al*., 2013], whereas, along the fault, the damage zone commonly enlarges in the direction of long-term fault propagation [e.g., *Manighetti et al*., 2004; *de Joussineau and Aydin*, 2007, 2009; *Schlagenhauf et al*., 2008; *Aydin and Berryman*, 2010; *Savage and Cooke*, 2010; *Faulkner et al*., 2011] (Figure 1b). Therefore, natural earthquakes rupture faults that are embedded in a predamaged medium, with this long-term damage having properties that vary both across and along the fault. Most available theoretical models take into account the predamaged state, yet consider that predamage is uniform along the fault [*Andrews*, 2005; *Ma*, 2008; *Templeton and Rice*, 2008; *Ma and Andrews*, 2010; *Kaneko and Fialko*, 2011; *Huang and Ampuero*, 2011; *Xu et al*., 2012b; *Gabriel et al*., 2013], at best varying across the fault [*Harris and Day*, 1997; *Ben-Zion and Huang*, 2002; *Ben-Zion and Shi*, 2005; *Rudnicki and Rice*, 2006; *Ampuero and Ben-Zion*, 2008; *Dunham and Rice*, 2008]. We suspect that this simplification might be one of the reasons of the discrepancy between model results and natural earthquake slip profiles.

In this paper, we explore how the predamaged state of the medium around a strike-slip fault can affect the slip distribution produced during an earthquake. In particular, we focus on the influence of the along-fault variations in the medium rigidity. Although we do not discuss the complexities or formation of fault damage, which is beyond the scope of this paper, we simulate the preexisting long-term damage and its "intensity," by decreasing the elastic modulus of the medium around the fault. Such a decrease in elastic moduli as damage increases has been observed on natural rocks and faults, both during and immediately after earthquake ruptures [*O'Connell and Budiansky*, 1974; *Li et al*., 1998, 2006; *Fialko et al*., 2002; *Vidale and Li*, 2003; *Ben-Zion et al*., 2003; *Fialko*, 2004] and around long-term geological faults [*Li et al*., 1990; *Gudmundsson*, 2004; *Faulkner et al*., 2006; *Aydin and Berryman*, 2010; *Barbot et al*., 2009; *Hearn and Fialko*, 2009; *Cochran et al*., 2009]. In that later case, damage is thus permanent [e.g., *Cochran et al*., 2009]. We then model the dynamic crack-like rupture of a slip-weakening planar fault and search which geometries and elastic properties of the long-term damage reproduce the characteristic triangular asymmetric slip profile on the earthquake rupture. We find that a generic earthquake slip profile is produced only when a laterally heterogeneous preexisting, long-term damage zone surrounds the ruptured fault. This arises from a significant part of the coseismic slip being diffused within the long-term damage zone.

2. Model Setup

We consider a 3-D planar, vertical strike-slip fault (30 × 15 km) embedded in an elastic medium whose properties vary spatially both across and along the fault (see below). The model is implemented in the finite difference code FLAC^{3D} [*Itasca Consulting Group*, 2006], which solves for elasto-dynamic wave propagation coupled to frictional sliding along the fault [*Cappa and Rutqvist*, 2012]. The code solves the equations of motion in a 3-D elastic medium

$$\rho \ddot{u}_i = \sigma_{ij,j} + f_i \tag{1}$$

$$\sigma_{ij} = \lambda u_{k,k} \delta_{i,j} + G\left(u_{i,j} + u_{j,i}\right) \tag{2}$$

where u is the displacement, σ is the stress tensor, f is the body force, ρ is the density of the medium, λ and G are Lame's constants, and δ is the Kronecker Delta. Einstein notation and summation over repeated indices are assumed. The double dot above u implies second-order differentiation with respect to time. The fault is modeled as an internal boundary using zero-thickness joint elements where the displacement can be discontinuous. Along the fault, a friction law governs the traction, which changes with respect to the initial stress. The evolution of friction with slip along the fault is described with a linear slip-weakening formulation [*Ida*, 1972; *Palmer and Rice*, 1973]; the friction coefficient (μ) depends on the amount of slip (D) and decays linearly from a peak static value (μ_s) down to a residual dynamic value (μ_d) over a critical slip distance (δ_o)

$$\mu = \begin{cases} \mu_s - (\mu_s - \mu_d)\dfrac{D}{\delta_o} & D < \delta_o \\ \mu_d & D > \delta_o \end{cases} \tag{3}$$

© 2014. American Geophysical Union. All Rights Reserved.

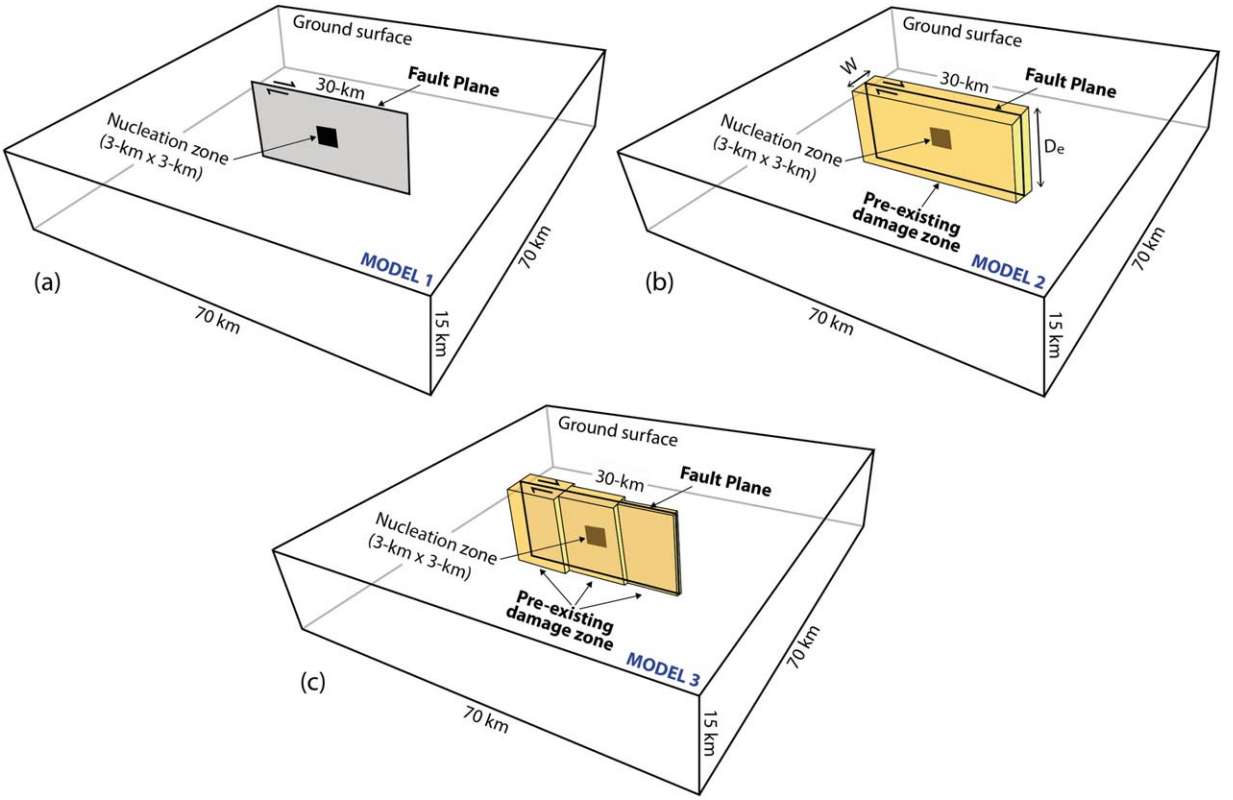

Figure 2. Model geometry: (a) fault plane (30 × 15 km) represented as a zero-thickness slip surface in a homogeneous elastic medium (elastic crack, Model 1); (b) same fault plane surrounded by a rectangular damage zone of constant width (W) along the entire depth (D_e) (Model 2); (c) same fault plane surrounded by a triangular damage zone fairly similar to that in Figure 1b (three zones of 10 km length each and of variable lateral widths along the entire depth) (Model 3). In all models, the damage zone extends over the entire depth and stops at the fault tips.

In the model, the shear strength of the fault is described as a function of the friction coefficient and the normal stress (σ_n)

$$\tau = \mu\sigma_n \tag{4}$$

The model domain has a lateral extension of 70 km and a depth of 15 km, the mean thickness of the seismogenic crust (Figure 2). This computational domain is limited laterally and at its base by absorbing conditions to avoid spurious wave reflections from boundaries. The 30 km long rupture plane where the coseismic slip occurs is represented by a zero-thickness interface (Figures 2a–2c). We surround this slip plane with a damage zone having different geometries and elastic properties (see below), extending over the entire depth of the model (depth extent of natural damage zones is poorly known, but might be large, extending across much of the brittle seismogenic crust [e.g., *Fialko et al*., 2002; *Li et al*., 2006; *Barbot et al*., 2009; *Cochran et al*., 2009; *Hearn and Fialko*, 2009; *Griffith et al*., 2012; *Smith et al*., 2013]), and stopping at the fault tips. We refer to the "damage width" in the direction perpendicular to the fault. The damage zone is embedded in a homogeneous elastic medium, referred to as the host rock (Young's modulus E_0 of 80 GPa, Poisson's ratio of 0.25, and density of 2670 kg/m^3). The damage zone is laterally discretized into three zones in order to accommodate variations in width and elastic properties along the fault strike. We simulate the degree of damage by different values of the Young's modulus in the damage zone (E_d), E_d decreasing as damage increases. We vary E_d in the range 10–70 GPa. The degree of rigidity contrast between the damage zone and the host rock is $\delta E/E_o = (E_0 - E_d)/E_0$. Consequently, $\delta E/E_o$ ranges from ~12 to 90%. This range is large enough to include realistic values; available prior works indeed estimate a rigidity reduction in damaged zones of 40–75% relative to the ambient crust [e.g., *Fialko et al*., 2002; *Katz et al*., 2003; *Gudmundsson*, 2004; *Hamiel and Fialko*, 2007; *Healy*, 2008; *Cochran et al*., 2009; *Barbot et al*., 2009; *Gudmundsson et al*., 2011; *Griffith et al*., 2012]. The variation in the Young's modulus encapsulates all the complex processes that

© 2014. American Geophysical Union. All Rights Reserved.

might contribute to the rock damage (i.e., plastic strain, crack activation and formation, macroscopic fault slip, poroelastic effects, etc. [see *Lyakhovsky et al*., 1997; *Dalguer et al*., 2003; *Manighetti et al*., 2004; *Andrews*, 2005; *Ando and Yamashita*, 2007; *Templeton and Rice*, 2008; *Ma and Andrews*, 2010; *Xu and Ben-Zion*, 2013), as well as those that might contribute to its variation over short times (such as postseismic healing [e.g., *Brantley et al*., 1990; *Moore et al*., 1994; *Vidale and Li*, 2003; *Schaff and Beroza*, 2004; *Brenguier et al*., 2008; *Mitchell and Faulkner*, 2009]). In other words, the Young's modulus in the modeled damage zone represents the finite, cumulative state of the damage well within the interseismic phase of the earthquake cycle that precedes the slip event that we consider.

The mesh size on the fault plane and in the damage zone is 50 m, while it increases gradually to 250 m toward the model boundaries. We submit the model to a homogeneous initial stress field with normal stress of 120 MPa and shear stress of 70 MPa [e.g., *Noda and Lapusta*, 2010; *Pelties et al*., 2012]. The stresses are applied inside the model and at the boundaries, although the top boundary is free to move (we have also tested constant displacement boundary conditions, and the results are unchanged). Note that we are not suggesting that uniform distribution of initial stress is characteristic of active faults. However, since natural earthquake slip profiles are generic regardless of their different stress contexts, we adopt this simplifying assumption.

The rupture nucleation is initiated by a shear stress value (81.6 MPa) higher than the fault strength in a 3 km long square patch centered both along-strike and along-dip at a depth of 7.5 km, a common centroid depth for crustal earthquakes [*Scholz*, 2002]. The fault is governed by linear slip-weakening friction (static friction μ_s of 0.677, dynamic friction μ_d of 0.525, and slip weakening distance δ_o of 0.4 m; commonly used parameters [e.g., *Harris et al*., 2009]). We compute the spontaneous rupture for a total duration of 20 s. The rupture behaves as an expanding crack-like slip zone, having a constant stress drop everywhere on the fault plane.

In such a theoretical framework, the elastic properties and geometry of the damage zone are expected to exert a strong control on the on-fault slip. Assuming linear elasticity, the fault strike-slip displacement (D) is [*Fialko et al*., 2002; *Duan et al*., 2011]

$$D = w\Delta\tau\left(\frac{1}{G_d} - \frac{1}{G_o}\right) \tag{5}$$

where w is the fault zone width, $\Delta\tau$ is the shear stress change, G_d is the shear modulus of the damage zone, and G_o is the shear modulus of the ambient intact rock

$$G_d = \frac{E_d}{2(1+\nu_d)} \tag{6}$$

$$G_o = \frac{E_o}{2(1+\nu_o)} \tag{7}$$

where E_d and ν_d are the Young's modulus and Poisson ratio of the damage zone, and E_o and ν_o are those of the ambient intact rock. Assuming that variations in the Poisson ratio are small compared with variations in the Young's modulus ($\nu \sim \nu_o \approx \nu_d$), combining equation (5) with equations (6) and (7) gives

$$D = 2(1+\nu)w\Delta\tau\left(\frac{E_o - E_d}{E_o E_d}\right) \tag{8}$$

From equations (3) and (4), the model assumes a constant shear stress change everywhere on the rupture plane. In such a context of constant $\Delta\tau$, equation (8) predicts that a fault embedded in a homogeneous medium (i.e., no damage) has an elliptical slip distribution, as shown in Figure 3. By contrast, the existence of a damage zone with low rigidity and/or large width around the rupture is predicted to yield an increase of the on-fault coseismic slip [*Barbot et al*., 2008].

We performed 82 simulations dedicated to explore those scaling relations, especially to examine the effects of the degree of damage and of the size of the damage zone on the resulting earthquake slip. Results are

© 2014. American Geophysical Union. All Rights Reserved.

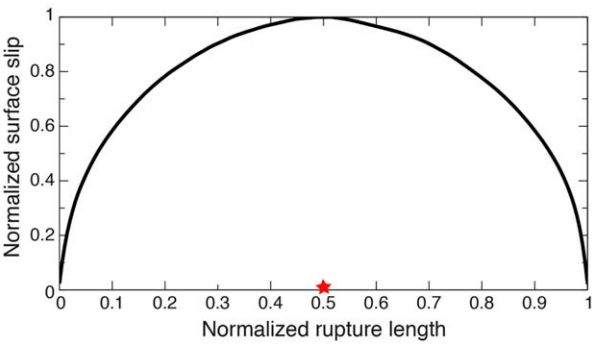

Figure 3. Calculated earthquake slip profile at the surface as a function of the rupture length (normalized) for the elastic crack model (Model 1; Figure 2a). The red star at the center of the horizontal axis is the position of the epicenter.

presented in two ways. We first show plots of the final on-fault coseismic slip (D, measured along the top boundary) normalized to the maximum slip of an elastic crack in homogeneous medium (D_0) (i.e., no damage; Figure 3), as a function of the normalized rupture length (Figures 4, 6, and 7). This dimensionless representation allows to examine the slip profile envelope shapes and to estimate the variation in on-fault slip compared to the reference crack model. Second, all the results are synthesized in diagrams where the rigidity contrast between the damage zone and the host rock ($\delta E/E_o$), the relative size of the damage zone (width to length ratio, W/L), and the produced maximum on-fault slip (normalized to the elastic crack solution, D/D_o) are plotted together (Figures 5 and 8). This representation allows us to examine and compare for a broad range of conditions the effects of the damage zone properties on the produced on-fault slip.

3. Model Results

3.1. Rectangular Shape Preexisting Damage Zone With Homogeneous Elastic Properties

We prescribe a preexisting damage zone with a rectangular shape around the slip plane and with homogeneous elastic properties (Figure 2b). This case is that prescribed in most available theoretical models, which consider that predamage is uniform along the fault [*Andrews*, 2005; *Ma*, 2008; *Templeton and Rice*, 2008; *Dunham and Rice*, 2008; *Ma and Andrews*, 2010; *Kaneko and Fialko*, 2011; *Huang and Ampuero*, 2011; *Xu et al*., 2012b; *Gabriel et al*., 2013]. We impose the damage zone to have different widths (W) ranging from ~3 to 50% of the fault length. It is important to note that, although it has long been supposed that damage was confined only within a very narrow zone around the faults [*Li et al*., 1998; *Ben-Zion et al*., 2003; *Fialko*, 2004; *Fielding et al*., 2009; *Mitchell and Faulkner*, 2009], an increasing number of observations suggests that it might rather extend over large areas up to several kilometers [*Spudich and Olsen*, 2001; *Manighetti et al*., 2004; *Oskin et al*., 2007; *Cochran et al*., 2009; *Barbot et al*., 2009; *Shelef and Oskin*, 2010; *Griffith et al*., 2012; *Smith et al*., 2013]. Several studies have suggested that the damage zone width might scale linearly with the fault length and/or displacement [*Scholz et al*., 1993; *Knott et al*., 1996; *Vermilye and Scholz*, 1998; *Beach et al*., 1999; *Manighetti et al*., 2004; *Savage and Brodsky*, 2011], but the actual ratios between damage zone width and fault length are still poorly known. The broad range of W/L ratios that we consider is thus made to insure that we capture realistic values. In each model, we prescribe a constant Young's modulus for the entire damage zone.

Figures 4a–4g show the modeled slip profiles obtained for variable width rectangular damage zones (width varied by 2 km steps) which have a Young's modulus of 70, 60, 50, 40, 30, 20, and 10 GPa, respectively; that is, a contrast in the Young's modulus between the damage zone and the host rock ($\delta E/E_o$) of ~12, 25, 37, 50, 62, 75, and 87%. In none of the tests a triangular slip profile is produced. Instead, the rupture slip profiles have an elliptical or roughly rectangular envelope shape. All the profiles are symmetric around the middle of the fault. The cases with stiffer damage actually resemble the elastic crack behavior. The amount of fault slip increases as the Young's modulus in the damage zone decreases. Meanwhile, the slip to length ratio of the profiles increases as the damage zone becomes wider (Table S1 in the supporting information). In the cases of a narrow, very compliant damage zone ($E_d = 10$ and 20 GPa), more stresses accumulate near the fault tips where they induce larger on-fault slip.

Figure 5 shows the combined effect of the elastic properties and of the relative width of the rectangular damage zone on the on-fault slip. The most compliant and the widest is the damage zone, the greatest is the maximum coseismic slip on the rupture. In narrow damage zones ($W/L \leq \sim 20$ %), E_d must be lower

© 2014. American Geophysical Union. All Rights Reserved.

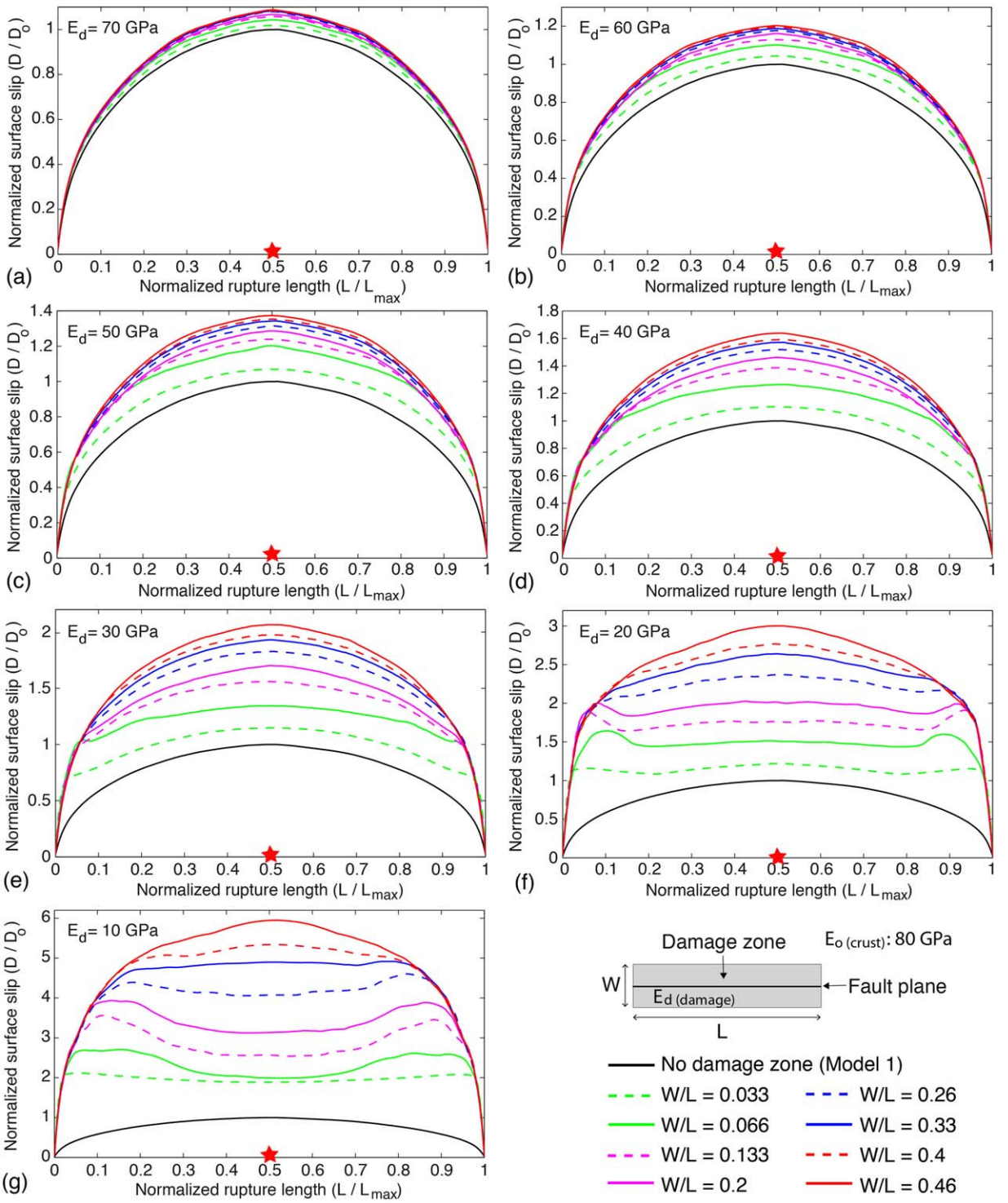

Figure 4. Calculated earthquake slip profiles at the surface as a function of the rupture length (normalized) for a fault surrounded by a rectangular damage zone (Model 2; Figure 2b). W: damage zone width; L: fault length. In each plot, the slip profiles (D) are normalized to the maximum slip (D_o) on the reference elastic crack (Figure 3). Results are presented for constant Young's modulus E_d in the damage zone, of (a) 70 GPa, (b) 60 GPa, (c) 50 GPa, (d) 40 GPa, (e) 30 GPa, (f) 20 GPa, and (g) 10 GPa. In each plot, the colors indicate the ratio of the width of the damage zone to fault length, as listed at the bottom of the graphs. The red star at the center of the horizontal axis is the position of the epicenter. The solution for the elastic crack model with no damage (Model 1; Figure 2a) is shown in black.

© 2014. American Geophysical Union. All Rights Reserved.

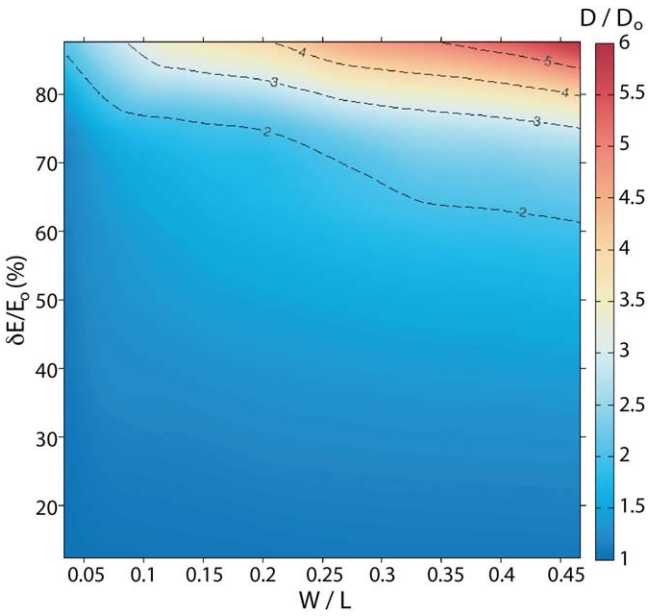

Figure 5. Diagram illustrating the combined effects of the contrast of Young's modulus between the damage zone (E_d) and the host rock (E_0) ($\delta E/E_o = (E_0 - E_d)/E_0$) and of the ratio of the damage zone width to fault length (W/L), on the maximum on-fault slip (D, normalized to the maximum slip (D_o) on the reference elastic crack) for the rectangular damage zone cases, presented in Figure 4 (i.e., with both constant Young's modulus E_d and constant damage zone width).

than ~20 GPa for the on-fault slip to markedly increase; in large damage zones (W/L ≥ ~30%), E_d values of ~30 GPa are enough to significantly increase the on-fault slip.

3.2. Rectangular Shape Preexisting Damage Zone With Laterally Varying Elastic Properties

Figure 6 presents the same simulations as before, yet with the rectangular damage zone having its Young's modulus increasing from right to left; that is, the intensity of damage decreases from right to left, while the damage zone width keeps constant along the fault. We have tested a case with a "rigid" damage zone (E_d = 70, 50, 40 GPa, Figure 6a) and another case with a more compliant damage zone (E_d = 40, 20, 10 GPa, Figure 6b). In the rigid damage zone (Figure 6a), the triangular slip profile is not produced. Instead, the rupture slip has a distorted elliptical shape whose asymmetry results from the maximum slip translating toward the less rigid part of the damage zone. In the compliant damage zone (Figure 6b), a triangular slip profile is produced, regardless of the damage zone width. The profiles are asymmetric with the maximum slip translated toward the right tip of the fault, around which damage is greatest, whereas slip linearly decreases toward the left fault tip, in the direction of damage decrease. Therefore, a high slip gradient develops near the limit between the softer damage zone and the host rock, whereas the gradient in slip decreases as the difference in modulus between damaged and host rocks decreases. The slip to length ratio of the profiles increases as the damage zone becomes wider (Table S1 in the supporting information). Because of the skewed shape of the profiles, the maximum slip lies away from the hypocenter.

The combined effects of the elastic properties and of the relative width of the rectangular damage zone on the on-fault slip are discussed in section 3.4.

3.3. Triangular Shape Preexisting Damage Zone With Homogeneous Elastic Properties

Field observations of long-term faults and related damage [*Shipton and Cowie*, 2001, 2003; *Kim et al*., 2004; *Manighetti et al*., 2004; *Dor et al*., 2006; *Faulkner et al*., 2011] (Figure 1b), as well as dynamic simulations of coseismic damage [e.g., *Andrews*, 2005; *Templeton and Rice*, 2008; *Viesca et al*., 2008; *Dunham et al*., 2011a, 2011b; *Xu et al*., 2012a, 2012b; *Xu and Ben-Zion*, 2013], suggest that damage zones around faults and ruptures commonly have an overall triangular shape in map view, with an apex centered in the zone of fault or rupture initiation, and a damage zone widening in the direction of fault or earthquake propagation (Figure 1b). Here we test the effect of an overall triangular-shaped preexisting damage zone of the form sketched in Figures 1b and 2c. Figure 7a shows the simulations with a damage zone widening from right to left along the fault, having constant elastic properties. None of the simulations produce the generic triangular shape of the earthquake slip profiles. Instead, the profiles have a quasi-elliptical shape when the difference in modulus between the damage zone and the host rock is low, and a fairly rectangular shape when the damage zone is soft (i.e., large contrast in Young's modulus). In that later case, a slight asymmetry develops in the slip distribution, as maximum slip translates toward the largest section of the compliant damage zone. Finally, the slip to length ratio of the profiles increases as the damage level increases (Table S1 in the supporting information).

© 2014. American Geophysical Union. All Rights Reserved.

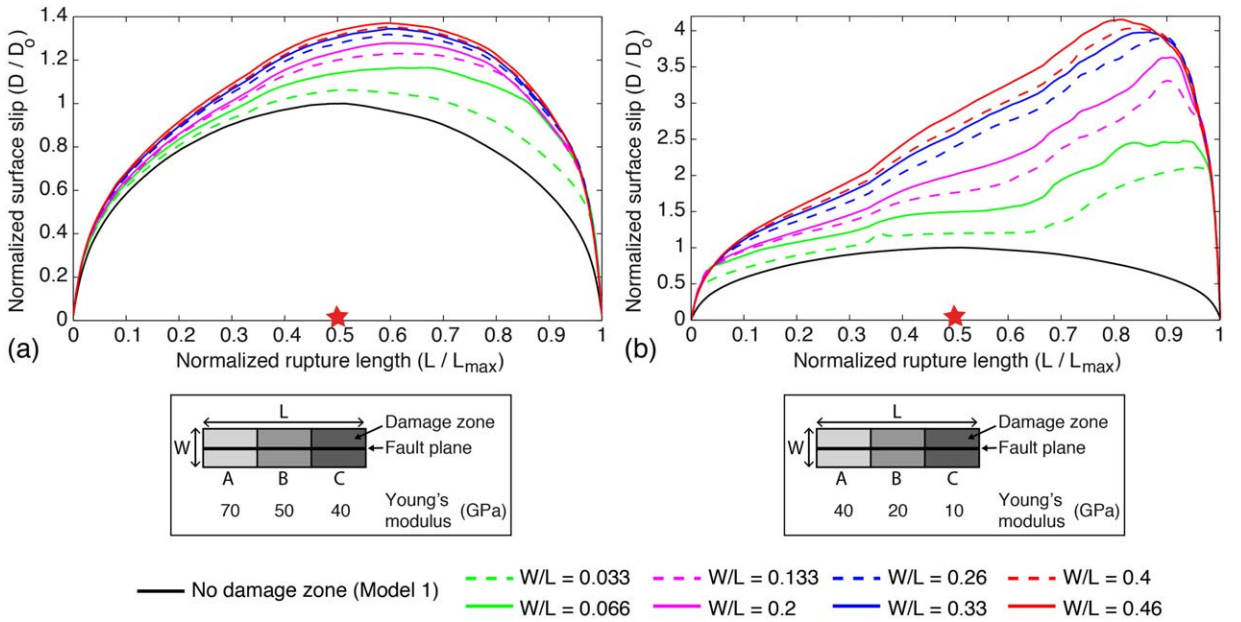

Figure 6. Calculated earthquake slip profiles at the surface as a function of the rupture length (normalized) for a fault surrounded by a rectangular damage zone (Model 2; Figure 2b). W: damage zone width; L: fault length. In each plot, the slip profiles (D) are normalized to the maximum slip (D_o) on the reference elastic crack (Figure 3). Results are presented for Young's modulus E_d decreasing from the left tip to the right tip along three zones (A, B, C, respectively), 10 km long each. (a) Case with a stiff damage zone. Young's modulus E_d is 70 GPa in zone A, 50 in zone B and 40 GPa in zone C. (b) Case with a compliant damage zone. Young's modulus E_d is 40 GPa in zone A, 20 in zone B, and 10 GPa in zone C. In each plot, the colors indicate the ratio of the width of the damage zone to fault length, as listed at the bottom of the graphs. The red star at the center of the horizontal axis is the position of the epicenter. For reference and comparison between results, the elastic crack model with no damage (Model 1; Figure 2a) is shown in black.

3.4. Triangular Shape Preexisting Damage Zone With Laterally Varying Elastic Properties

Figure 7b presents the same simulations as before, yet now with the damage zone having a Young's modulus increasing from right to left (from 10 to 40 GPa); that is, the intensity of damage decreases from right to left, as the damage zone width increases along the fault. Three different width increases are tested, from 1 to 3 km (W/L up to 10%, in green), from 2 to 6 km (W/L up to 20%, in blue), and from 4 to 12 km (W/L up to 40%, in magenta). All calculations produce a triangular, asymmetric earthquake slip profile, with maximum slip translated toward the right tip of the fault, far away from the rupture hypocenter. The slip then decreases roughly linearly from its maximum value to almost zero at the other (left) tip of the fault. The slip to length ratio of the profiles increases as the damage zone becomes wider, yet in a moderate fashion since all three calculated ratios basically remain in the similar range $\sim$4–6.5 $\times$ 10^{-4} (Table S1 in the supporting information).

Figure 7c presents the same calculations as before, yet for a damage zone whose Young's modulus now decreases from right to left (from 40 to 10 GPa) as the damage zone becomes wider. We thus prescribe here a preexisting damage that both enlarges and intensifies from right to left along the fault. The calculation is performed for a damage zone width varying from 4 to 12 km from right to left and is compared to the result obtained previously with the same damage zone geometry and opposite Young's modulus variation (magenta profile in Figures 7b and 7c). The resulting slip profile is triangular and asymmetric, yet tapering in the opposite direction to that of the previous simulation (Figure 7b). The maximum slip is thus translated toward the left tip of the fault, still away from the hypocenter. The slip to length ratio of the resulting slip profile is of the same order to the one obtained in the opposite configuration (magenta profile), yet slightly larger.

Figure 8 shows the combined effect of the elastic properties and of the relative width of the damage zone on the maximum on-fault slip, in the cases where one or both of the elastic properties and the width of the damage zone vary along fault strike. Those cases thus include the rectangular (Figure 6) and the triangular damage zones (Figures 7a and 7b). To account for the along-strike variation in W_d and E_d, we represent the

© 2014. American Geophysical Union. All Rights Reserved.

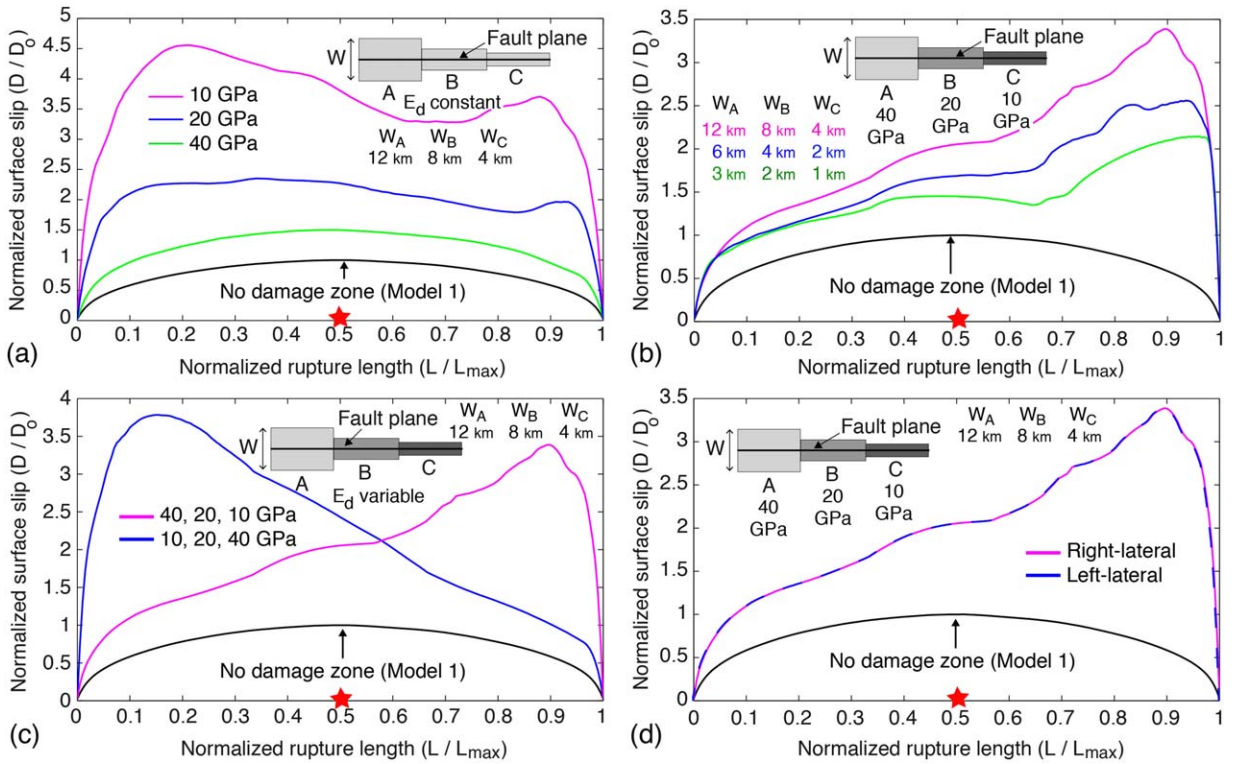

Figure 7. Calculated earthquake slip profiles at the surface as a function of the rupture length (normalized) for (a) a fault zone with a damage zone of variable width (regions A, B, C of similar length from left fault tip to right fault tip and of width $W_A = 12$ km, $W_B = 8$ km, $W_C = 4$ km) and constant Young's modulus E_d (magenta curve: 10 GPa, blue curve: 20 GPa, green curve: 40 GPa) (Model 3; Figure 2c); (b) a fault with a damage zone of variable width (from 1 to 3 km in green, from 2 to 6 km in blue, and from 4 to 12 km in magenta) and variable Young's modulus E_d (region A in light gray: 40 GPa, region B in gray: 20 GPa, and region C in dark gray: 10 GPa); (c) a Young's modulus E_d in the damage zone decreasing (blue) and increasing (magenta) in the direction of increasing damage zone width; and (d) modeled slip profiles on right-lateral (magenta) and left-lateral (blue) ruptures. The damage zone width ranges from 4 to 12 km for results presented in Figures 7c and 7d. In each plot, the slip profiles (D) are normalized to the maximum slip (D_o) on the reference elastic crack (Figure 3). The red star at the center of the horizontal axis is the position of the epicenter. For reference and comparison between results, the elastic crack model with no damage (Model 1; Figure 2a) is shown in black.

average damage width and elastic modulus. The presence of the damage zone significantly increases the maximum on-fault coseismic slip (compared to the reference crack model) whenever the damage is compliant overall, with an average Young's modulus lower than ~40 GPa. There is a tradeoff, however, between the average width and the compliance of the damage zone; while narrow damage zones must be compliant to yield a significant increase in coseismic slip, wider damage zones can be stiffer (average $E_d \sim 40$ GPa) and still produce significant on-fault slip increase. A damage zone with an average Young's modulus between ~20 and 40 GPa results in the earthquake rupture accumulating increased slip, which accrues as the damage zone widens overall. When the damage zone is very compliant, with average E_d between ~15 and 20 GPa, the on-fault slip markedly increases, although at a slower rate than in cases of stiffer damage zones. This probably results from a significant part of the slip being accommodated within the compliant damage zone. Figure 8 suggests that an increase in on-fault slip might dramatically occur in the cases of extremely compliant damage zones (average $E_d < 10$–15 GPa), but those cases are probably unrealistic (i.e., the rock would be completely destroyed).

3.5. Influence of the Sense of Lateral Slip

Figure 7d shows the same calculation as in Figure 7b (right to left width increase from 4 to 12 km, magenta curve), but with a rupture that is now imposed to be left lateral. The governing equations of the model predict invariance of slip magnitude with respect to direction of slip propagation. We verify that the model indeed produces this invariance. The resulting slip profile is exactly the same, showing that, in the chosen damage configuration (i.e., triangular-shaped, enlarging from right to left and decreasing in intensity from right to left) and under the present model assumptions, the sense of fault slip has no influence on the final shape of the coseismic slip profile.

© 2014. American Geophysical Union. All Rights Reserved.

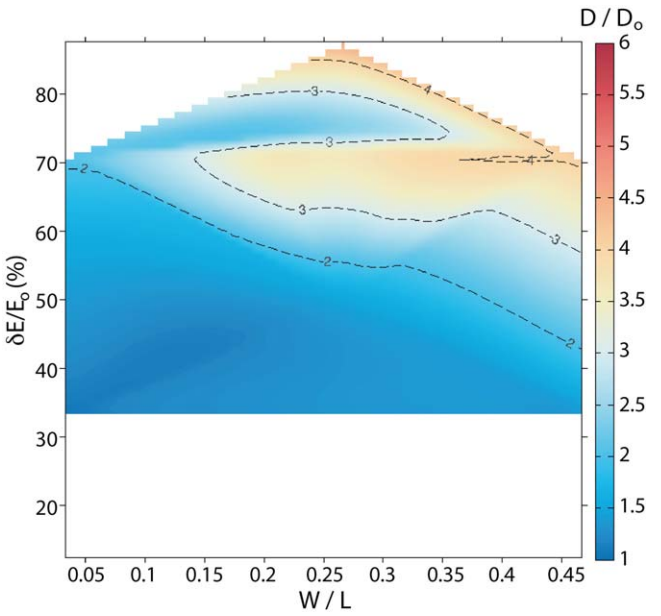

Figure 8. Diagram illustrating the combined effects of the contrast of Young's modulus between the damage zone (E_d) and the host rock (E_0) ($\delta E/E_o = (E_0 - E_d)/E_0$) and of the ratio of the damage zone width to fault length (W/L), on the maximum on-fault slip (D, normalized to the maximum slip (D_o) on the reference elastic crack) for the heterogeneous cases, i.e., with variable Young's modulus E_d and constant or variable damage zone width (rectangular and triangular damage zone cases, presented in Figures 6 and 7a–7c). To account for the along-strike variation in W_d and E_d, we represent the average damage width and elastic modulus. See discussion in text.

4. Discussion

In the absence of any preexisting damage in the medium surrounding a fault, the rupture of that fault produces an elliptical slip profile, far different from the slip distributions observed on natural earthquakes. Models simulating faults and earthquakes in homogeneous, linear, elastic medium are thus inappropriate to reproduce the natural earthquakes.

Our models suggest that the map view geometry of preexisting damage is not a major controlling factor for earthquake slip distributions; whatever the geometry of long-term damage (in the range tested here, from rectangular to triangular), the formed coseismic slip profiles are far different from being triangular if the damage elastic properties are uniform within the damage zone. Therefore, theoretical models that embed a fault within a predamaged medium with uniform properties are expected to be inappropriate in reproducing slip profiles for natural earthquakes. This finding also suggests that the width of the long-term damage zones might be variable, and not necessarily scaling with the fault length.

The factor most controlling the earthquake slip distributions seems to be the along-fault variability in the elastic properties of the preexisting damage. Note that a similar finding has been suggested for long-term, cumulative slip profiles [*Bürgmann et al*., 1994; *Manighetti et al*., 2004]. We discuss further below the possible nature of long-term damage and the reasons for its lateral variability. Whatever these reasons, we find that a progressive change in the elastic properties of the preexisting damage is a sufficient condition to account for the development of a generic, triangular, and asymmetric coseismic slip profile on the ruptured fault. The average elastic properties of the damage zone must be fairly compliant however (see Figure 6a where an average E_d value of ~55 GPa does not produce a triangular profile). In those conditions, the generic slip profile forms regardless of the width (from very small (i.e., W/L ~3%) to very large (W/L ~50%)) and of the geometry (rectangular or triangular) of the preexisting damage zone. Although other factors might contribute to shape the coseismic slip profiles, such as heterogeneous loading of the fault, lithological properties of the surrounding rocks, variable friction on the fault, local stress interactions, nonplanar fault geometry, etc. [e.g., *Bürgmann et al*., 1994; *Cooke*, 1997; *Manighetti et al*., 2001; *Martel and Shacat*, 2006], the generic, scale and context-independent envelope shape of the natural earthquake slip distributions shows that the role of those possible additional factors is not dominant.

The existence of a preexisting heterogeneous damage zone markedly affects the slip on the ruptured fault; whatever the damage geometry, the coseismic slip is larger on the fault section surrounded by the most intense damage, whereas the coseismic slip is decreased on the fault sections surrounded by stiffer damage (Figures 6b, 7b, and 8). There is a tradeoff however between the average width and the compliance of the damage zone; the stiffer the damage zone, the wider it must be to increase the on-fault coseismic slip. On the contrary, a narrow damage zone (i.e., W/L < ~10%) can yield a marked increase in the on-fault coseismic slip provided that it is compliant (average E_d < 20–30 GPa). Additionally, for a similar average Young's

© 2014. American Geophysical Union. All Rights Reserved.

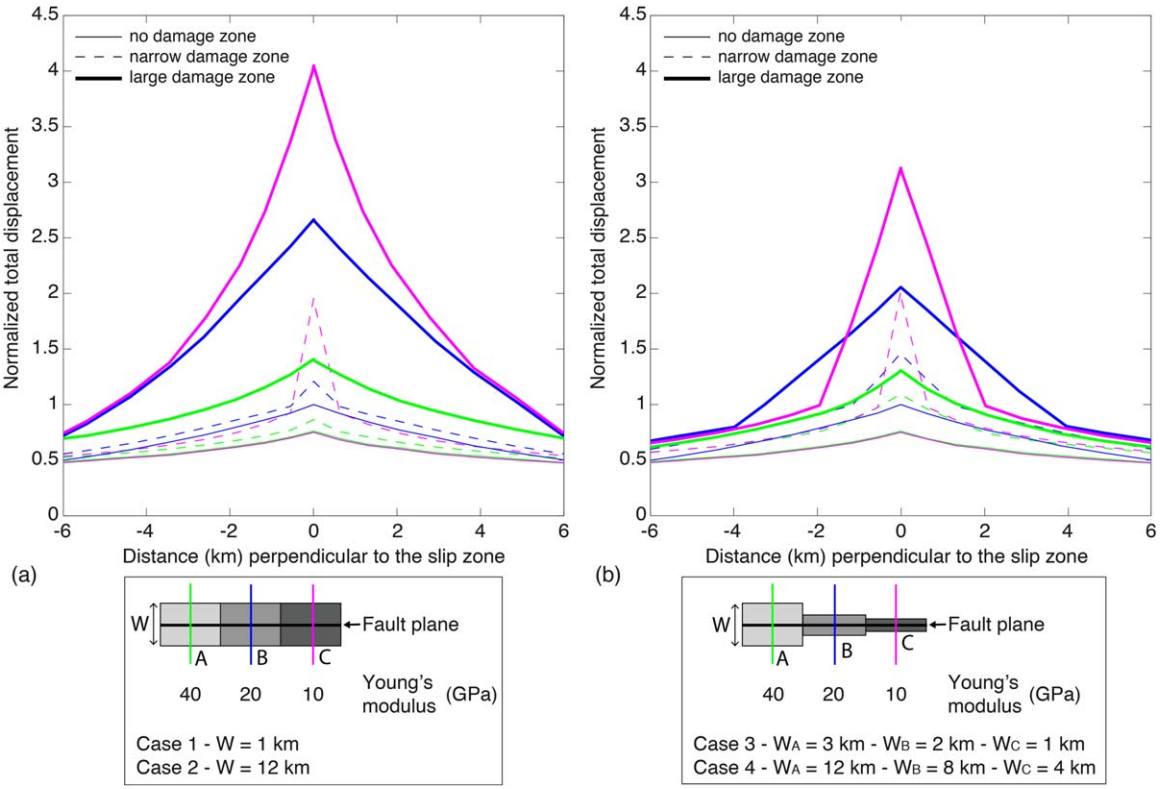

Figure 9. Total displacement (normalized to the maximum slip (D_o) on the reference elastic crack) measured perpendicular to the fault (located at the position "0" on the horizontal axis) along three transects in the models with (a) a rectangular (Model 2; Figure 2b) and (b) a triangular (Model 3; Figure 2c) damage zone. Inset: magenta line crosses the more compliant region of the damage zone (10 GPa), blue line the intermediate region (20 GPa), and green line the stiffer damage region (40 GPa). Solid lines correspond to the models with the largest damage zone, named cases 2 and 4: (a) W = 12 km, (b) W_A = 12 km, W_B = 8 km, W_C = 4 km, and dashed lines correspond to the models with the narrowest damage zones, named cases 1 and 3: (a) W = 1 km, (b) W_A = 3 km, W_B = 2 km, W_C = 1 km. The elastic crack solution with no damage is shown by the thin solid line. Maximum slip on the elastic crack is <1 because the transects are at some distance from D_0. Off-slip values measured at the center of the damage zone (i.e., at middistance between the fault and the damage outer edge) are reported in Table 2 of the supporting information.

modulus E_d in the range 20–30 GPa, a damage zone with laterally varying elastic properties can produce a larger coseismic on-fault slip (Figure 8) compared to a damage zone with constant elastic properties (Figure 5).

In addition to on-fault slip, a significant part of the coseismic slip is accommodated within the preexisting damage zone. We estimate the off-fault slip amount in the center of the damage zone at three different sites along the fault, and for four different damage geometries (noted cases 1–4 in Figure 9 and Table S2 in the supporting information). In each case, the off-fault slip is in the range 23–76% of the maximum on-fault slip, implying an independence from the damage zone geometry. The amount of off-fault slip relative to the maximum on-fault slip decreases as damage becomes stiffer, in all cases by ~40–60% with respect to values in the most compliant parts of the damage zone. However, as on-fault slip decreases in the direction of damage stiffening, the proportion of off-fault to on-fault slip (on same transect) slightly increases in all cases but case 4 (from ~75 to ~90% in the narrowest damage zones [cases 1 and 3], and from ~40 to ~65% in the widest case 2 damage zone); that is, a greater proportion of the local on-fault slip is diffused in the stiffer parts of the damage zone. Within the narrowest damage zones (cases 1 and 3), 60–75% of the maximum on-fault slip is accommodated in the areas where damage is high to moderate, while this amount decreases down to ~40% in the areas of stiffer damage. Within the widest damage zones (cases 2 and 4), 40–60% of the maximum on-fault slip is accommodated in areas of high to moderate damage, while this amount decreases down to ~25% in the areas where damage is stiffer. Therefore, these results show that a large amount of slip and hence strain is dissipated within the long-term damage zone, of at least ~25–40% (relative to maximum on-fault slip) and on average ~50%. We further discuss those off-fault slip amounts below.

© 2014. American Geophysical Union. All Rights Reserved.

In the case where coseismic slip profiles are strongly dependent on the along-fault properties of preexisting damage, the generic triangular shape of slip profiles is produced regardless of the sense of slip of the rupture; if the fault is right-lateral or left-lateral, the coseismic slip is always largest on the fault section which is surrounded by the greatest preexisting damage, and decreases where the fault is surrounded by stiffer preexisting damage.

These findings suggest that the zone of largest coseismic slip does not necessarily correlate with the location of the earthquake hypocenter, in keeping with observations of natural earthquakes [*Manighetti et al*., 2005]. Furthermore, the direction of coseismic slip tapering does not necessarily indicate the direction of rupture propagation, as observed in several natural earthquakes (such as Landers 1992, Chi-Chi 1999, and Denali 2002).

Finally, the slip-to-length ratios of the modeled slip profiles are in the range of natural earthquake slip-to-length ratios, albeit slightly larger (Table S1 in the supporting information) [*Manighetti et al*., 2007]. This suggests our modeling approach is too simple to reproduce all the features of natural earthquakes.

We thus show that the predamaged state of the medium that surrounds the earthquake faults must be taken into account to reproduce the observed generic envelope shape of the coseismic slip profiles. As said earlier, this does not preclude other factors might further influence the shape of the earthquake slip functions, as suggested in both theoretical dynamic models (i.e., preearthquake stress on the fault, ambient stress, variability in fault static and dynamic friction [e.g., *Rice et al*., 2005; *Wolf et al*., 2006; *Xu and Ben-Zion*, 2013; *Noda et al*., 2013]) and fault mechanics analyses [e.g., *Bürgmann et al*., 1994; *Cooke*, 1997; *Martel and Shacat*, 2006].

We also show that the predamaged state of the medium must be heterogeneous along the fault for an earthquake slip profile to develop a triangular and asymmetric shape. The lateral variation of cumulative damage along the faults is a well-known feature. Most faults are indeed flanked (on one or both sides) by a damaged, generally highly fractured zone. Whether those damage zones are formed only by the stress concentrations around the propagating rupture fronts [*Scholz et al*., 1993] or also include relicts of the long-term fault growth process through segment linkage and quasi-static fault slip [*Manighetti et al*., 2004] remains unresolved [*Dunham et al*., 2011a, 2011b; *Savage and Brodsky*, 2011]. Furthermore, whether the damage process dominantly includes microcrack activation and/or formation [*Lyakhovsky et al*., 1997; *Yamashita*, 2000; *Dalguer et al*., 2003; *Manighetti et al*., 2004; *Suzuki*, 2012], macroscopic shear faulting [*Ando and Yamashita*, 2007], or plasticity [*Andrews*, 2005; *Ben-Zion and Shi*, 2005; *Templeton and Rice*, 2008; *Viesca et al*., 2008; *Duan and Day*, 2008; *Ma and Andrews*, 2010; *Dunham et al*., 2011a, 2011b; *Xu and Ben-Zion*, 2013; *Gabriel et al*., 2013] also remains unresolved. Whatever the nature of the cumulative damage around the faults, the across-fault width of the long-term damage zone seems to increase as the fault lengthens laterally over time [*Scholz et al*., 1993; *Manighetti et al*., 2004; *Kim et al*., 2004; *Faulkner et al*., 2011; *Savage and Brodsky*, 2011]. The enlargement of the damage zone with rupture lengthening is also suggested in most dynamic simulations [e.g., *Andrews*, 2005; *Templeton and Rice*, 2008; *Savage and Cooke*, 2010; *Xu and Ben-Zion*, 2013]. Additionally, cumulative damage is most intense around the most ancient sections of the fault which have slipped over longer time spans and decreases in intensity (i.e., increase in Young's modulus) in the direction of fault lengthening, that is, in the direction in which the fault becomes younger (Figure 1b). This leads to laterally varying cumulative damage along fault with commensurate lateral variations in elastic properties.

Earthquake faults are intrinsically embedded in a predamaged, heterogeneous medium, whose properties are likely to influence the dynamics of the next events. The predamaged zones will define the zones where the dynamic stresses might be more efficiently dissipated, with this dissipation in turn controlling the velocity of the rupture propagation and the amount of coseismic slip on the earthquake fault [*Harris and Day*, 1997; *Ben-Zion and Andrews*, 1998; *Ampuero and Ben-Zion*, 2008; *Barbot et al*., 2008]. Damage might also introduce some asymmetry between the two fault compartments and hence contribute to the "bimaterial situation" described in several theoretical models [*Andrews and Ben-Zion*, 1997; *Ben-Zion and Huang*, 2002; *Shi and Ben-Zion*, 2006; *Bhat et al*., 2007; *Biegel et al*., 2008; *Dunham and Rice*, 2008; *Ampuero and Ben-Zion*, 2008].

As in other prior works [e.g., *Barbot et al*., 2008; *Dunham et al*., 2011a, 2011b], we find that the coseismic slip is increased on the fault section that is surrounded with most intense cumulative damage. That specific fault

© 2014. American Geophysical Union. All Rights Reserved.

section represents the most mature part of the fault, where the fault has accumulated greater slip. Since our calculations are performed with homogeneous friction on the fault, one possible explanation for the slip increase on the most mature fault section is that the strong reduction of elastic moduli in the damage zone leads to a significant coseismic motion amplification [*Spudich and Olsen*, 2001; *Shi and Ben-Zion*, 2006]. As the damage level decreases along the fault, such a positive feedback decreases, resulting in a decrease of slip on the ruptured fault. Whatever the amount of slip on the earthquake fault, and whatever the geometry of the damage zone, a significant part of the coseismic slip, at least 25–40% of the maximum on-fault slip, is diffused in the damage zone.

Since the modeled coseismic slips are greatest on the fault sections surrounded with most mature damage, we would expect earthquakes on long-lived mature faults to have larger slip to length ratios than events produced on young, immature faults. The slip to length ratios of ~250 natural earthquakes worldwide show the opposite; the most mature faults produce earthquakes with the lowest slip to length ratio [*Kanamori and Anderson*, 1975; *Shaw and Scholz*, 2001; *Scholz*, 2002; *Manighetti et al*., 2007]. A possible factor contributing to this apparent paradox is that modeled slip amounts are not robustly constrained and so the models are too simple to properly reproduce the entire set of earthquake properties. In particular, we impose nucleation stresses that might be too large compared to the actual stresses required for natural earthquake slip. A second element comes from the observation that most large earthquakes, especially those on mature faults, rupture several major segments along a fault [e.g., *Manighetti et al*., 2007]. Fault segments are connected with geometrical features such as offsets, kinks, and bends, which may produce local changes of stress and strength. Earthquakes should thus be modeled as multisegments ruptures [e.g., *Kagan*, 2004; *Manighetti et al*., 2007, 2009], not as single faults as we have done here, and as most available models do. Furthermore, as a fault accumulates more slip and hence becomes more mature, it is likely that the static and dynamic frictions on the fault plane evolve and probably decrease [e.g., *Cooke*, 1997]. The variability of fault friction with fault maturity is therefore another parameter that should be included in earthquake slip models and that might also explain the slip to length ratio paradox. In this study, we use a fairly high static friction of $\mu_s \sim 0.7$, that might be more appropriate to simulate the behavior of fairly immature faults [e.g., *Cooke*, 1997].

Since our modeling produces earthquake slip to length values which are slightly greater than natural data [e.g., *Manighetti et al*., 2007], we may expect that the actual degree of off-fault slip might be lower than the values we have inferred from our models. However the amount of off-fault slip must still be significant to explain the natural earthquake slip profiles. *Chester et al*. [2005] and *Wilson et al*. [2005] found that a large part of the earthquake energy budget (possibly up to 50%) must be diffused within the damage zone to account for the fracture surface area in this zone.

Finally, our models suggest that off-fault coseismic slip and strain can occur at large distances away from the fault, up to a distance of several tens of percent of the fault length in the tested models; for the 30 km long fault modeled here, the average width of the damage zone might thus be up to several kilometers. The narrowest damage zones in our study have a W/L ratio of a few percent, which correspond to damage zone widths of 1–2 km, similar to those revealed in recent studies [e.g., *Cochran et al*., 2009]. Our modeling suggests that the width of the damage zone can either vary or stay constant along the fault trace. Therefore, it is not clear that a scaling relation is to be expected between damage zone width and fault length or displacement [*Savage and Brodsky*, 2011].

5. Conclusions

Our modeling results provide new insights on the influence of preexisting long-term damage around active faults on the earthquake slip distribution. The preexisting damage encapsulates a long-term record of inelastic deformation associated with the earthquake cycles and the possible quasi-static growth of the fault over geological time. It manifests as a relative compliance of the off-fault medium with respect to the ambient crust. Here we show that elastic heterogeneities associated with variations in damage intensity of the medium along the fault exert a significant control on the earthquake slip distribution. Our model, with along-fault variations in the elastic modulus of the long-term damage zone, successfully predicts the observed generic, triangular envelope shape of natural coseismic slip profiles. The model that best explains these earthquake slip profiles suggests that the fault experiences the highest slip across the most compliant

© 2014. American Geophysical Union. All Rights Reserved.

section of the damage zone, while the coseismic slip decreases as the damage stiffness increases. However, whether damage is high or low, the off-fault coseismic slip is high in the damage zone, at least 25–40% of the maximum on-fault coseismic slip (in the center of the damage zone). Since our modeling produces earthquake slip to length values which are slightly greater than those for natural events [e.g., *Manighetti et al*., 2007], we may expect that actual off-fault slip amounts might be slightly lower than the inferred values. However, they still must be significant to explain the natural earthquake slip profiles. Finally, our models also suggest that off-fault coseismic slip and strain can occur at large distances away from the fault, up to a distance of several tens of percent of the fault length in the tested models, equivalent to several kilometers for a 30 km long fault.

Together with prior works, our results suggest that significant inelastic deformation occurs in the "near" field of faults and of earthquake ruptures. Paradoxically, the theory of elasticity lays the foundation for nearly every aspect of our understanding of earthquake source mechanics [e.g., *Aki and Richards*, 2002; *Ma and Andrews*, 2010]. Our results, along with others before [*Barbot et al*., 2008, 2009; *Cochran et al*., 2009; *Kaneko and Fialko*, 2011], therefore motivate a reinterpretation and/or reformulation of the available earthquake source inversion models since most of them do not include inelastic deformation occurring in the volume around the earthquake ruptures (inversion models including damage have only been developed recently to model interseismic slip [see *Barbot et al*., 2013]).

Our work confirms that triangular asymmetric coseismic slip profiles can emerge from natural fault behaviors and geometries. The generic triangular shape of the earthquake slip profiles has critical implications on the earthquake stress drop, as the later cannot be constant on the fault under common assumptions (see more detailed discussion in *Noda et al*. [2013]). The coseismic slip tapering also suggests that significant strain and stress redistributions occur during an earthquake event, probably in a fairly large zone around the ruptured fault. This might have important implications on how stress is transferred, and therefore on seismic hazard assessment.

Acknowledgments
This work was supported by the Observatoire de la Côte d'Azur through the "BQR OCA." We thank Thorsten Becker, Tom Mitchell, Sylvain Barbot, and Michele Cooke for their constructive reviews and useful suggestions, which greatly helped us to improve our manuscript. We also thank James Hollingsworth for his careful reading of the paper and his thorough comments.

References

Aki, K., and P. G. Richards (2002), *Quantitative Seismology*, 2nd ed., pp. 339, Univ. Sci. Books, Sausalito, Calif.
Ando, R., and T. Yamashita (2007), Effects of mesoscopic-scale fault structure on dynamic earthquake ruptures: Dynamic formation of geometrical complexity of earthquake faults, *J. Geophys. Res.*, *112*, B09303, doi:10.1029/2006JB004612.
Andrews, D. J., and Y. Ben-Zion (1997), Wrinkle-like slip pulse on a fault between different materials, *J. Geophys. Res.*, *102*(B1), 553–571.
Andrews, D. J. (2005), Rupture dynamics with energy loss outside the slip zone, *J. Geophys. Res.*, *81*, B01307, doi:10.1029/2004JB003191.
Ampuero, J.-P., and Y. Ben-Zion (2008), Cracks, pulses and macroscopic asymmetry of dynamic rupture on a bimaterial interface with velocity-weakening friction, *Geophys. J. Int.*, *173*, 674–692, doi:10.1111/j.1365-246X.2008.03736.x.
Aydin, A., and J. G. Berryman (2010), Analysis of the growth of strike-slip faults using effective medium theory, *J. Struct. Geol.*, *32*(11), 1629–1642, doi:10.1016/jsg.2009.11.007.
Barbot, S., Y. Fialko, and D. Sandwell (2008), Effect of a compliant fault zone on the inferred earthquake slip distribution, *J. Geophys. Res.*, *113*, B06404, doi:10.1029/2007JB005256.
Barbot, S., Y. Fialko, and D. Sandwell (2009), Three-dimensional models of elasto-static deformation in heterogeneous media, with application to the Eastern California Shear Zone, *Geophys. J. Int.*, *179*, 500–520,doi:10.1111/j.1365-246X.2009.04194.x.
Barbot, S., P. Agram, and M. De Michele (2013), Change of apparent segmentation of the San Andreas fault around Parkfield from space geodetic observations across multiple periods, *J. Geophys. Res.*, *118*, 6311–6327, doi:10.1002/2013JB010442.
Beach, A., A. I. Welbon, P. J. Brockbank, and J. E. McCallum (1999), Reservoir damage around faults: Outcrop examples from the Suez rift, *Pet. Geosci.*, *5*(2), 109–116, doi:10.1144/petgeo.5.2.109.
Ben-Zion, Y., and D. J. Andrews (1998), Properties and implications of dynamic rupture along a material interface, *Bull. Seismol. Soc. Am.*, *88*(4), 1085–1094.
Ben-Zion, Y., and Y. Huang (2002), Dynamic rupture on an interface between a compliant fault zone layer and a stiffer surrounding solid, *J. Geophys. Res.*, *107*(B2), 2042, doi:10.1029/2001JB000254.
Ben-Zion, Y., Z. Peng, D. Okaya, L. Seeber, L. G. Armbruster, N. Ozer, A. J. Michael, S. Baris, and M. Aktar (2003), A shallow fault zone structure illuminated by trapped waves in the Karadere-Duzce branch of the North Anatolian Fault, western Turkey, *Geophys. J. Int.*, *152*, 699–717, doi:10.1046/j.1365-246X.2003.01870.x.
Ben-Zion, Y., and Z. Shi (2005), Dynamic rupture on a material interface with spontaneous generation of plastic strain in the bulk, *Earth Planet. Sci. Lett.*, *236*, 486–496.
Bhat, H. S., R. Dmowska, G. C. P. King, Y. Klinger, and J. R. Rice (2007), Off-fault damage patterns due to supershear ruptures with application to the 2001 Mw 8.1 Kokoxili (Kunlun) Tibet earthquake, *J. Geophys. Res.*, *112*, B06301, doi:10.1029/2006JB004425.
Bhat, H., R. L. Biegel, A. J. Rosakis, and C. G. Sammis (2010), The effect of asymmetric damage on dynamic shear rupture propagation II: With mismatch in bulk elasticity, *Tectonophysics*, *493*(3), 263–271, doi:10.1016/j.tecto.2010.03.016.
Biegel, R. L., C. G. Sammis, and A. J. Rosakis (2008), An experimental study of the effect of off-fault damage on the velocity of a slip pulse, *J. Geophys. Res.*, *113*, B04302, doi:10.1029/2007JB005234.
Biegel, R. L., H. S. Bhat, C. G. Sammis, and A. J. Rosakis (2010), The effect of asymmetric damage on dynamic shear rupture propagation I: No mismatch in bulk elasticity, *Tectonophysics*, *493*(3), 254–262, doi:10.1016/j.tecto.2010.03.020.

© 2014. American Geophysical Union. All Rights Reserved.

Brantley, S. L., B. Evans, S. H. Hickman, and D. A. Crerar (1990), Healing of microcracks in quartz—Implications for fluid-flow, *Geology*, *18*(2), 136–139.
Brenguier, F., M. Campillo, C. Hadziioannou, N. M. Shapiro, R. M. Nadeau, and E. Larose (2008), Postseismic relaxation along the San Andreas fault at Parkfield from continuous seismological observations, *Science*, *321*, 1478–1481, doi:10.1126/science.1160943.
Bürgmann, R., D. D. Pollard, and S. J. Martel (1994), Slip distributions on faults: Effects of stress gradients, inelastic deformation, heterogeneous host-rock stiffness, and fault interaction, *J. Struct. Geol.*, *16*(12), 1675–1690.
Cappa, F., and J. Rutqvist (2012), Seismic rupture and ground accelerations induced by CO_2 injection in the shallow crust, *Geophys. J. Int.*, *190*, 1784–1789, doi:10.1111/j.1365-246X.2012.05606.x.
Chester, J. S., F. M. Chester, and A. K. Kronenberg (2005), Fracture surface energy of the Punchbowl fault, San Andreas system, *Nature*, *437*, 133–136.
Chester, F. M., and J. S. Chester (1998), Ultracataclasite structure and friction processes of the Punchbowl, San Andreas system, California, *Tectonophysics*, *295*, 199–221, doi:10.1016/S0040-1951(98)00121-8.
Chester, F. M., and J. M. Logan (1986), Implications for mechanical-properties of brittle faults from observations of the Punchbowl Fault Zone, California, *Pure Appl. Geophys.*, *124*, 79–106.
Cochran, E. S., Y. G. Li, P. M. Shearer, S. Barbot, Y. Fialko, and J. E. Vidale (2009), Seismic and geodetic evidence for extensive, long-lived fault damage zones, *Geology*, *37*, 315–318, doi:10.1130/G25306A.1.
Cooke, M. L. (1997), Fracture localization along faults with spatially varying friction, *J. Geophys. Res.*, *102*(B10), 22,425–22,434, doi:10.1029/97JB01829.
Dahlen, F. A. (1977), The balance of energy in earthquake faulting, *Geophys. J. R. Astron. Soc.*, *48*, 239–261.
Dalguer, L. A., K. Irikura, and J. D. Riera (2003), Simulation of tensile crack generation by three-dimensional dynamic shear rupture propagation during an earthquake, *J. Geophys. Res.*, *108*(B3), 2144, doi:10.1029/2001JB001738.
de Joussineau, G., and A. Aydin (2007), The evolution of the damage zone with fault growth in sandstone and its multiscale characteristics, *J. Geophys. Res.*, *112*, B12401, doi:10.1029/2006JB004711.
de Joussineau, G., and A. Aydin (2009), Segmentation of strike-slip faults revisited, *Pure Appl. Geophys.*, *166*(10), 1575–1594, doi:10.1007/s00024-009-0511-4.
Dieterich, J. H., and D. E. Smith (2009), Nonplanar faults: Mechanics of slip and off-fault damage, *Pure Appl. Geophys.*, *166*, 1799–1815.
Dor, O., T. K. Rockwell, and Y. Ben-Zion (2006), Geological observations of damage asymmetry in the structure of the San Jacinto, San Andreas and Punchbowl faults in Southern California: A possible indicator for preferred rupture propagation direction, *Pure Appl. Geophys.*, *163*(2–3), 301–349, doi:10.1007/s00024-005-0023-9.
Dor, O., C. Yildirim, T. K. Rockwell, Y. Ben-Zion, O. Emre, M. Sisk, and T. Y. Duman (2008), Geologic and geomorphologic asymmetry across the rupture zones of the 1943 and 1944 earthquakes on the North Anatolian Fault: Possible signals for preferred earthquake propagation direction, *Geophys. J. Int.*, *173*, 483–504, doi:10.1111/j.1365-246X.2008.03709.x.
Duan, B., and S. M. Day (2008), Inelastic strain distribution and seismicitv radiation from rupture of a fault kink, *J. Geophys. Res.*, *113*, B12311, doi:10.1029/2008JB005847.
Duan, B., J. Kang, and Y. G. Li (2011), Deformation of compliant fault zones induced by nearby earthquakes: Theoretical investigations in two dimensions, *J. Geophys. Res.*, *116*, B03307, doi:10.1029/2010JB007826.
Dunham, E., and J. R. Rice (2008), Earthquake slip between dissimilar poroelastic materials, *J. Geophys. Res.*, *113*, B09304, doi:10.1029/2007JB005405.
Dunham, E. M., D. Belanger, L. Cong, and J. E. Kozdon (2011a), Earthquake ruptures with strongly rate-weakening friction and off-fault plasticity. 1: Planar faults, *Bull. Seismol. Soc. Am.*, *101*(5), 2296–2307, doi:10.1785/0120100075.
Dunham, E. M., D. Belanger, L. Cong, and J. E. Kozdon (2011b), Earthquake ruptures with strongly rate-weakening friction and off-fault plasticity. 2: Nonplanar faults, *Bull. Seismol. Soc. Am.*, *101*(5), 2308–2322, doi:10.1785/0120100076.
Faulkner, D. R., T. M. Mitchell, D. Healy, and M. Heap (2006), Slip on 'weak' faults by the rotation of regional stress in the fracture damage zone, *Nature*, *444*(7121), 922–925.
Faulkner, D. R., T. M. Mitchell, E. Jensen, and J. Cembrano (2011), Scaling of fault damage zones with displacement and the implications for fault growth processes, *J. Geophys. Res.*, *116*, B05403, doi:10.1029/2010JB007788.
Fialko, Y., D. Sandwell, D. Agnew, M. Simons, P. Shearer, and B. Minster (2002), Deformation on nearby faults induced by the 1999 Hector Mine earthquake, *Science*, *297*, 1858–1862, doi:10.1126/science.1074671.
Fialko, Y. (2004), Probing the mechanical properties of seismically active crust with space geodesy: Study of the co-seismic deformation due to the 1992 Mw7.3 Landers (southern California) earthquake, *J. Geophys. Res.*, *109*, B03307, doi:10.1029/2003JB002756.
Fielding, E. J., P. Lundgren, R. Bürgmann, and G. J. Funning (2009), Shallow fault-zone dilatancy recovery after the 2003 Bam earthquake in Iran, *Nature*, *458*, 64–68, doi:10.1038/nature07817.
Finzi, Y., E. H. Hearn, Y. Ben-Zion, and V. Lyakhovsky (2009), Structural properties and deformation patterns of evolving strike-slip faults: Numerical simulations incorporating damage rheology, *Pure Appl. Geophys.*, *166*, 1537–1573, doi:10.1007/s00024-009-0522-1.
Gabriel, A., J. P. Ampuero, L. A. Dalguer, and P. M. Mai (2013), Source properties of dynamic rupture pulses with off-fault damage, *J. Geophys. Res.*, *118*, 4117–4126, doi:10.1002/jgrb.50213.
Griffith, W. A., S. Nielsen, G. Di Toro, and S. A. F. Smith (2010), Rough faults, distributed weakening, and off-fault deformation, *J. Geophys. Res.*, *115*, B08409, doi:10.1029/2009JB006925.
Griffith, W. A., T. M. Mitchell, J. Renner, and G. Di Toro (2012), Coseismic damage and softening of fault rocks at seismogenic depths, *Earth Planet. Sci. Lett.*, *353–354*, 219–230.
Gudmundsson, A. (2004), Effects of Young's modulus on fault displacement, *C. R. Geosci.*, *336*, 85–92.
Gudmundsson, A., T. H. Simmenes, B. Larsen, and S. L. Philipp (2011), Effects of internal structure and local stresses on fracture propagation, deflection, and arrest in fault zones, *J. Struct. Geol.*, *32*, 1643–1655.
Hamiel, Y., and Y. Fialko (2007), Structure and mechanical properties of faults in the North Anatolian Fault system from InSAR observations of coseismic deformation due to the 1999 Izmit (Turkey) earthquake, *J. Geophys. Res.*, *112*, B07412, doi:10.1029/2006JB004777.
Harris, R. A., and S. M. Day (1997), Effects of a low-velocity zone on a dynamic rupture, *Bull. Seismol. Soc. Am.*, *87*(5), 1267–1280.
Harris, R., et al. (2009), The SCEC/USGS Dynamic Earthquake Rupture Code verification exercise, *Seismol. Res. Lett.*, *80*(1), 119–126, doi:10.1785/gssrl.80.1.119.
Healy, D. (2008), Damage patterns, stress rotations and pore fluid pressures in strike-slip fault zones, *J. Geophys. Res.*, *113*, B12407, doi:10.1029/2008JB005655.
Hearn, E. H., and Y. Fialko (2009), Can compliant fault zones be used to measure absolute stresses in the upper crust?, *J. Geophys. Res.*, *114*, B04403, doi:10.1029/2008JB005901.

© 2014. American Geophysical Union. All Rights Reserved.

Hok, S., M. Campillo, F. Cotton, P. Favreau, and I. Ionescu (2010), Off-fault plasticity favors the arrest of dynamic ruptures on strength heterogeneity: Two-dimensional cases, *Geophys. Res. Lett.*, *37*, L02306, doi:10.1029/2009GL041888.
Huang, Y., and J.-P. Ampuero (2011), Pulse-like ruptures induced by low-velocity fault zones, *J. Geophys. Res.*, *116*, B12307, doi:10.1029/2011JB008684.
Ida, Y. (1972), Cohesive force across the tip of a longitudinal-shear crack and Griffith's specific surface energy, *J. Geophys. Res.*, *77*(20), 3796–3805.
Itasca Consulting Group (2006), *FLAC^{3D}, Fast Lagrangian Analysis of Continua in 3 Dimensions*, Version 3.0, Itasca Consult. Group, Minneapolis, Minn.
Kagan, Y. Y. (2004), Short-term properties of earthquake catalogs and models of earthquake source, *Bull. Seismol. Soc. Am.*, *94*(4), 1207–1228, doi:10.1785/012003098.
Kanamori, H., and D. L. Anderson (1975), Theoretical basis of some empirical relations in seismology, *Bull. Seismol. Soc. Am.*, *65*(5), 1073–1095.
Kanamori, H., and L. Rivera (2006), Energy partitioning during an earthquake, in *Earthquakes: Radiated Energy and the Physics of Faulting, Geophys. Monogr. Ser.*, edited by R. Abercrombie, A. McGarr, G. Di Toro, H. Kanamori, vol. 170, pp. 3–13, AGU, Washington, D. C.
Kaneko, Y., and Y. Fialko (2011), Shallow slip deficit due to large strike-slip earthquakes in dynamic rupture simulations with elasto-plastic off-fault response, *Geophys. J. Int.*, *186*, 1389–1403.
Katz, O., Z. Reches, and G. Baer (2003), Faults and their associated host rock deformations: Part I. Structure of small faults in a quartz-syenite body, southern Israel, *J. Struct. Geol.*, *25*, 1675–1689.
Kim, Y. S., D. C. P. Peacock, and S. J. Sanderson (2004), Fault damage zones, *J. Struct. Geol.*, *26*, 503–517.
Knott, S. D., A. Beach, P. J. Brockbank, J. L. Brown, J. E. McCallum, and A. I. Welbon (1996), Spatial and mechanical controls on normal fault populations, *J. Struct. Geol.*, *18*(2–3), 359–372, doi:10.1016/S0191-8141(96)80056-3.
Kostrov, B. V. (1974), Seismic moment and energy of earthquakes, and seismic flow of rock, *Izv. Earth Phys.*, *1*, 23–40.
Li, Y. G., P. Leary, K. Aki, and P. Malin (1990), Seismic trapped modes in the Oroville and San Andreas fault zones, *Science*, *249*, 763–766.
Li, Y. G., J. E. Vidale, K. Aki, F. Xu, and T. Burdette (1998), Evidence of shallow fault zone strengthening after the 1992 M7.5 Landers, California, earthquake, *Science*, *279*, 217–219, doi:10.1126/science.279.5348.217.
Li, Y. G., P. Chen, E. S. Cochran, J. E. Vidale, and T. Burdette (2006), Seismic evidence for rock damage and healing on the San Andreas Fault associated with the 2004 M 6.0 Parkfield earthquake, *Bull. Seismol. Soc. Am.*, *96*(4B), S349–S363.
Lyakhovsky, V., Y. Ben-Zion, and A. Agnon (1997), Distributed damage, faulting, and friction, *J. Geophys. Res.*, *102*(B12), 27,635–27,649.
Ma, S. (2008), A physical model for widespread near-surface and fault zone damage induced by earthquakes, *Geochem. Geophys. Geosyst.*, *9*, Q11009, doi:10.1029/2008GC002231.
Ma, S., and D. J. Andrews (2010), Inelastic off-fault response and three-dimensional dynamics of earthquake rupture on a strike-slip fault, *J. Geophys. Res.*, *115*, B04304, doi:10.1029/2009JB006382.
Manighetti, I., G. King, Y. Gaudemer, C. H. Scholz, and C. Doubre (2001), Slip accumulation and lateral propagation of active normal faults in Afar, *J. Geophys. Res.*, *106*(B7), 13,667–13,669.
Manighetti, I., G. King, and C. G. Sammis (2004), The role of off-fault damage in the evolution of normal faults, *Earth Planet. Sci. Lett.*, *217*, 399–408.
Manighetti, I., M. Campillo, C. G. Sammis, P. M. Mai, and G. King (2005), Evidence for self-similar, triangular slip distributions on earthquakes: Implications for earthquake and fault mechanics, *J. Geophys. Res.*, *110*, B05302, doi:10.1029/2004JB003174.
Manighetti, I., M. Campillo, S. Bouley, and F. Cotton (2007), Earthquake scaling, fault segmentation, and structural maturity, *Earth Planet. Sci. Lett.*, *253*, 429–438, doi:10.1016/j.epsl.2006.11.004.
Manighetti, I., D. Zigone, M. Campillo, and F. Cotton (2009), Self-similarity of the largest-scale segmentation of the faults: Implications for earthquake behavior, *Earth Planet. Sci. Lett.*, *288*(3–4), 370–381, doi:10.1016/j.epsl.2009.09.040.
Martel, S. J., and C. Shacat (2006), Mechanics and interpretations of fault slip, *AGU Geophys. Monogr. Ser.*, *170*, 207–215.
Mitchell, T. M., and D. R. Faulkner (2009), The nature and origin of off-fault damage surrounding strike-slip fault zones with a wide range of displacements: A field study from the Atacama fault system, northern Chile, *J. Struct. Geol.*, *31*, 802–816, doi:10.1016/j.jsg.2009.05.002.
Moore, D. E., D. A. Lockner, and J. D. Byerlee (1994), Reduction of permeability in granite at elevated-temperatures, *Science*, *265*(5178), 1558–1561.
Ngo, D., Y. Huang, A. J. Rosakis, W. A. Griffith, and D. D. Pollard (2012), Off-fault tensile cracks: A link between geological fault observations, lab experiments and dynamic rupture models, *J. Geophys. Res.*, *117*, B01307, doi:10.1029/2011JB008577.
Noda, H., and N. Lapusta (2010), Three-dimensional earthquake sequence simulations with evolving temperature and pore pressure due to shear heating: Effect of heterogeneous hydraulic diffusivity, *J. Geophys. Res.*, *115*, B12314, doi:10.1029/2010JB007780.
Noda, H., N. Lapusta, and H. Kanamori (2013), Comparison of average stress drop measures for ruptures with heterogeneous stress change and implications for earthquakes physics, *Geophys. J. Int.*, *193*(3), 1691–1712, doi:10.1093/gji/ggt074.
O'Connell, R. J., and B. Budiansky (1974), Seismic velocities in dry and saturated cracked solids, *J. Geophys. Res.*, *79*(35), 5412–5426.
Oskin, M. E., K. Le, and M. D. Strane (2007), Quantifying fault-zone activity in arid environments with high-resolution topography, *Geophys. Res. Lett.*, *34*, L23S05, doi:10.1029/2007GL031295.
Palmer, A. C., and J. R. Rice (1973), Growth of slip surfaces in progressive failure of over-consolidated clay, *Proc. R. Soc. London, Ser. A*, *332*(1591), 527–548.
Pelties, C., J. de la Puente, J. P. Ampuero, G. B. Brietzke, and M. Käser (2012), Three dimensional dynamic rupture simulation with a high-order discontinuous Galerkin method on unstructured tetrahedral meshes, *J. Geophys. Res.*, *117*, B02309, doi:10.1029/2011JB008857.
Poliakov, A. N. B., R. Dmowska, and J. R. Rice (2002), Dynamic shear rupture interactions with fault bends and off-axis secondary faulting, *J. Geophys. Res.*, *107*(B11), 2295, doi:10.1029/2001JB000572.
Rice, J. R., C. Sammis, and R. Parsons (2005), Off-fault secondary failure induced by a dynamic slip pulse, *Bull. Seismol. Soc. Am.*, *95*, 109–134.
Rudnicki, J. W., and J. R. Rice (2006), Effective normal stress alteration due to pore pressure changes induced by dynamic slip propagation on a plane between dissimilar materials, *J. Geophys. Res.*, *111*, B10308, doi:10.1029/2006JB004396.
Sammis, C. G., A. J. Rosakis, and H. S. Bhat (2009), Effects of off-fault damage on earthquake rupture propagation: Experimental studies, *Pure Appl. Geophys.*, *166*, 1629–1648, doi:10.1007/s00024-009-052-3.
Savage, H. M., and E. E. Brodsky (2011), Collateral damage: Evolution with displacement of fracture distribution and secondary fault strands in fault damage zones, *J. Geophys. Res.*, *116*, B03405, doi:10.1029/2010JB007665.
Savage, H. M., and M. L. Cooke (2010), Unlocking the effects of friction on fault damage zones, *J. Struct. Geol.*, *32*, 1732–1741, doi:10.1016/j.jsg.2009.08.014.
Schaff, D. P., and G. C. Beroza (2004), Coseismic and postseismic velocity changes measured by repeating earthquakes, *J. Geophys. Res.*, *109*, B10302, doi:10.1029/2004JB003011.

© 2014. American Geophysical Union. All Rights Reserved.

Schlagenhauf, A., I. Manighetti, J. Malavieille, and S. Dominguez (2008), Incremental growth of normal faults: Insights from a laser-equipped analog experiment, *Earth Planet. Sci. Lett.*, *273*, 299–311, doi:10.1016/j.epsl.2008.06.042.
Scholz, C. H., N. H. Dawers, J. Z. Yu, M. H. Anders, and P. A. Cowie (1993), Fault growth and fault scaling laws: Preliminary results, *J. Geophys. Res.*, *98*(B12), 21,951–21,961.
Scholz, C. H. (2002), *The Mechanics of Earthquakes and Faulting*, 2nd ed., 471 p., Cambridge Univ. Press, Cambridge, Mass.
Shaw, B. E., and C. H. Scholz (2001), Slip-length scaling in large earthquakes: Observations and theory and implications for earthquake physics, *Geophys. Res. Lett.*, *28*(15), 2995–2998.
Shelef, E., and M. Oskin (2010), Deformation processes adjacent to active faults: Examples from eastern California, *J. Geophys. Res.*, *115*, B05308, doi:10.1029/2009JB006289.
Shi, Z., and Y. Ben-Zion (2006), Dynamic rupture on a bi-material interface governed by slip-weakening friction, *Geophys. J. Int.*, *165*, 469–484, doi:10.1111/j.1365-246X.2006.02853.x.
Shi, Z., A. Needleman, and Y. Ben-Zion (2010), Slip modes and partitioning of energy during dynamical frictional sliding between identical elastic-viscoplastic solids, *Int. J. Fract.*, *162*, 51–67, doi:10.1007/s10704-009-9388-6.
Shipton, Z., and P. A. Cowie (2001), Damage zone and slip surface evolution over μm to km scales in high-porosity Navajo sandstone, Utah, *J. Struct. Geol.*, *23*, 1825–1844.
Shipton, Z., and P. A. Cowie (2003), A conceptual model for the origin of fault damage zone structures in high-porosity sandstone, *J. Struct. Geol.*, *25*, 333–344.
Sibson, R. H. (2003), Thickness of the seismic slip zone, *Bull. Seismol. Soc. Am.*, *93*, 1169–1178.
Smith, S. A. F., A. Bistacchi, T. M. Mitchell, S. Mittempergher, and G. Di Toro (2013), The structure of an exhumed intraplate seismogenic fault in crystalline basement, *Tectonophysics*, *599*, 29–44, doi:10.1016/j.tecto.2013.03.031.
Spudich, P., and K. B. Olsen (2001), Fault zone amplified waves as possible seismic hazard along the Calaveras fault central California, *Geophys. Res. Lett.*, *28*(13), 2533–2536.
Suzuki, T. (2012), Understanding of dynamic earthquake slip behavior using damage as a tensor variable: Microcrack distribution, orientation, and mode and secondary faulting, *J. Geophys. Res.*, *117*, B05309, doi:10.1029/2011JB008908.
Templeton, E. L., and J. R. Rice (2008), Off-fault plasticity and earthquake rupture dynamics: 1. Dry materials or neglect of fluid pressure changes, *J. Geophys. Res.*, *13*, B09306, doi:10.1029/2007JB005529.
Tinti, E., P. Spudich, and M. Cocco (2005), Earthquake fracture energy inferred from kinematic rupture models on extended faults, *J. Geophys. Res.*, *110*, B12303, doi:10.1029/2005JB003644.
Vermilye, J. M., and C. H. Scholz (1998), The process zone: A microstructural view of fault growth, *J. Geophys. Res.*, *103*(B6), 12,223–12,237.
Vidale, J. E., and Y. G. Li (2003), Damage to the shallow Landers fault from the nearby Hector Mine earthquake, *Nature*, *421*(6922), 524–526.
Viesca, R. C., E. L. Templeton, and J. R. Rice (2008), Off-fault plasticity and earthquake rupture dynamics: 2. Effects of fluid saturation, *J. Geophys. Res.*, *113*, B09307, doi:10.1029/2007JB005530.
Wechsler, N., T. K. Rockwell, and Y. Ben-Zion (2009), Application of high resolution DEM data to detect rock damage from geomorphic signals along the central San Jacinto Fault, *Geomorphology*, *113*, 82–96, doi:10.1016/j.geomorph.2009.06.007.
Wilson, B., T. Dewers, Z. E. Reches, and J. Brune (2005), Particle size and energetics of gouge from earthquake rupture zones, *Nature*, *434*(7034), 749–752.
Wolf, S., I. Manighetti, M. Campillo, and I. R. Ionescu (2006), Mechanics of normal fault networks subject to slip-weakening friction, *Geophys. J. Int.*, *165*, 677–691, doi:10.1111/j.1365-246X.2006.02910.x.
Xu, S., Y. Ben-Zion, and J.-P. Ampuero (2012a), Properties of inelastic yielding zones generated by in-plane dynamic ruptures: I. Model description and basic results, *Geophys. J. Int.*, *191*, 1325–1342, doi:10.1111/j.1365-246X.2012.05679.x.
Xu, S., Y. Ben-Zion, and J.-P. Ampuero (2012b), Properties of inelastic yielding zones generated by in-plane dynamic ruptures: II. Detailed parameter-space study, *Geophys. J. Int.*, *191*, 1343–1360, doi:10.1111/j.1365-246X.2012.05685.x.
Xu, S., and Y. Ben-Zion (2013), Numerical and theoretical analyses of in-plane dynamic rupture on a frictional interface and off-fault yielding patterns at different scales, *Geophys. J. Int.*, *193*, 304–320, doi:10.1093/gij/ggs105.
Yamashita, T. (2000), Generation of microcracks by dynamic shear rupture and its effects on rupture growth and elastic wave radiation, *Geophys. J. Int.*, *143*, 395–406.

© 2014. American Geophysical Union. All Rights Reserved.